Eur. Phys. J. D **43**, 23–26 (2007)
DOI: 10.1140/epjd/e2007-00061-5

THE EUROPEAN PHYSICAL JOURNAL D

Photodissociation spectroscopy of the chromium trimer ion

T. Majima[1], K. Tono[1,a], A. Terasaki[2], Y. Kawazoe[3], and T. Kondow[2,b]

[1] East Tokyo Laboratory, Genesis Research Institute, Inc., 717-86 Futamata, Ichikawa, Chiba 272-0001, Japan
[2] Cluster Research Laboratory, Toyota Technological Institute, in East Tokyo Laboratory, Genesis Research Institute, Inc., 717-86 Futamata, Ichikawa, Chiba 272-0001, Japan
[3] Institute for Materials Research, Tohoku University, Sendai 980-77, Japan

Received 23 July 2006 / Received in final form 15 November 2006
Published online 24 May 2007 –

Abstract. The electronic and geometric structures and photodissociation dynamics of the chromium trimer ion, Cr_3^+, were investigated by photodissociation spectroscopy in the photon-energy range from 1.32 to 5.52 eV. The branching fractions of the product ions, Cr^+ and Cr_2^+, exhibit stepwise changes at the threshold energies for dissociation into Cr^++Cr_2, Cr+Cr_2^+, Cr^++2Cr, and Cr^*+Cr_2^+. It is noted that Cr_2^+ is produced even above the threshold for atomization; the excess energy is redistributed to produce a fragment atom, Cr^*, in an excited state. The photodissociation action spectrum is well explained by a mixture of simulated spectra for two nearly-degenerate structural isomers identified by density functional calculations: those having a metastable C_{2v} structure and the most stable structure slightly distorted from the C_{2v} one. The barrier height between the two isomers which is lower than the zero-point energy suggests that Cr_3^+ has an intrinsically floppy structure.

PACS. 36.40.Mr Spectroscopy and geometrical structure of clusters – 36.40.Qv Stability and fragmentation of clusters – 36.40.Cg Electronic and magnetic properties of clusters

1 Introduction

The chromium atom has the highest spin moment (6 μ_B) among the 3d transition metals due to the half-filled 3d and 4s electronic shells. In contrast, the dimer, Cr_2, forms a singlet state ($^1\Sigma_g^+$) in the ground state as a result of a covalent bond formation through delocalized 4s and 3d electrons; a portion of 3d electrons localized on each atomic site couples in an antiferromagnetic manner [1–6]. For the trimer, antiferromagnetic coupling between three Cr spins causes frustration in an equilateral triangle structure. An isolated trimer may easily relax the spin frustration by changing its geometrical structure. Therefore, a Cr trimer provides a good model to clarify the relationship between the spin coupling and geometrical structures. The structure of the neutral Cr trimer, Cr_3, is reported by the density-functional theory (DFT) in the level of the local spin density functional approximation (LSD) [7]. It is suggested that the Cr_3 is composed of a dimer and an atom interacting weakly with each other, in accordance with the dimer growth model proposed for small clusters up to Cr_{11}.

In this report, firstly, the electronic spectrum of Cr_3^+ obtained by the photodissociation spectroscopy is presented, which shows characteristic changes in the photodissociation process depending on the excitation photon energy. Secondly, theoretical calculations are presented, which include geometry optimization by the DFT calculation and simulation of the optical spectrum by the time-dependent density-functional theory (TD-DFT). The experimental results are analyzed on the basis of the geometric and electronic structures of Cr_3^+ provided by the DFT calculations.

2 Experimental studies

2.1 Experimental procedures

The experimental method has been described in detail elsewhere [8]. Chromium cluster ions were generated by the laser-vaporization technique with a helium carrier gas. The second harmonics of a pulsed Nd:YAG laser operated at 10 Hz was focused on a Cr disk. The temperature of the cluster-growth room was kept at room temperature. The cluster ions thus produced were extracted into a time-of-flight (TOF) mass spectrometer by a pulsed electric voltage of 1.6 kV. Trimer ions were mass-selected and irradiated with a tunable laser pulse from an optical parametric oscillator (OPO; MOPO-HF, Spectra Physics). The photon energy was varied from 1.32 through 5.52 eV with an interval of 0.02 eV. Note that there are instrumental

[a] *Present address:* Department of Chemistry, Faculty of Science, Tokyo University of Science, Kagurazaka, Shinjuku, Tokyo 162-8601, Japan.
[b] e-mail: kondow@clusterlab.jp

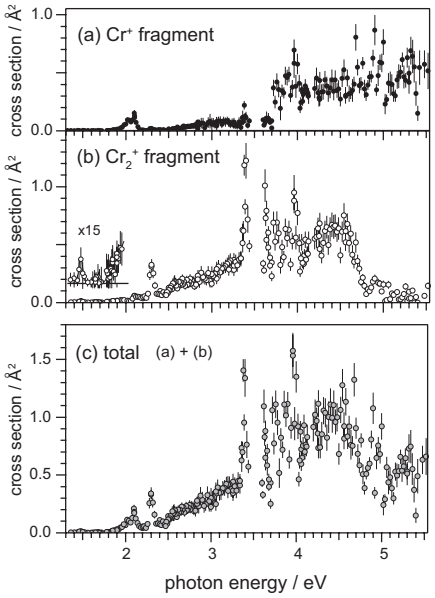

Fig. 1. Photodissociation cross sections of Cr_3^+. Partial cross sections for production of (a) Cr^+ and (b) Cr_2^+. (c) The total cross section obtained by adding the partial cross sections together. Error bars indicate statistical errors.

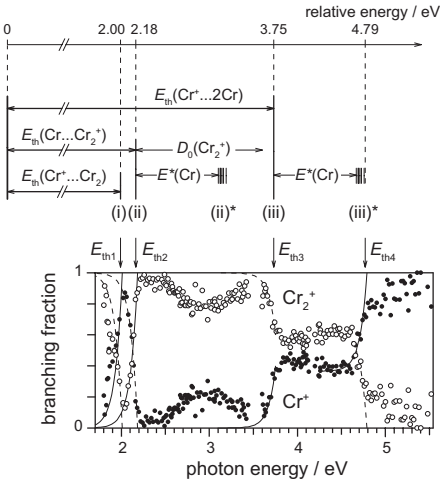

Fig. 2. Branching fractions for production of Cr^+ and Cr_2^+ as a function of the photon energy along with an energy-level diagram of photodissociation processes of Cr_3^+.

tuning gaps of the laser between 1.72 and 1.80 eV and between 3.44 and 3.60 eV. The laser line width is less than 0.03 meV. The photofragment ions and the residual primary ions were further mass-analyzed at 13 μs after photoexcitation by the secondary TOF mass-spectrometer equipped with a reflectron. A partial photodissociation cross section, σ_i, was obtained through the following relationship: $\sigma_i = D_i/\eta F$, where D_i is the intensity ratio of the ith fragment ion (I_i) to the sum of all the ions ($I_{\rm parent}+\Sigma I_i$), η is the ratio of the laser-interaction volume in the ion bunch to its entire volume, and F is the photon flux. The energy of the laser pulse was adjusted in the range of 0.2–8 mJ to keep the sum of D_i below 10% for holding the linear relationship between σ_i and D_i. The value of η was estimated to be 0.28 based on the assumption of Gaussian profiles for the laser and the ion beam.

2.2 Results of experiments

Figure 1 shows spectra of partial and total photodissociation cross sections of Cr_3^+. As shown in Figure 1a, Cr^+ production is observed above 1.8 eV with peaks discernible around 2.0–2.1 eV. It shows stepwise increase at about 3.7 eV and keeps similar cross sections up to 5.5 eV. Production of Cr_2^+ starts at about 1.9 eV. Note that Cr_2^+ ions observed below 1.9 eV were produced by two-photon absorption. It shows a broad structure between 1.9 and 4.8 eV; several narrow peaks were observed as well at 2.3 eV and in the 3.3–4.0-eV range.

Figure 2 shows branching fractions for production of specific fragment ions as a function of the photon energy. Stepwise changes are discernible at four excitation energies as indicated by arrows. An abrupt change in the branching fraction generally indicates a new predissociation channel. The onset behavior of each step in the branching fraction was analyzed as follows to obtain a threshold energy, $E_{\rm th}$, for each predissociation channel [8,9]: it is presumed that the onset takes place in a finite energy range because of the internal energy stored in the primary ions Cr_3^+. Provided that the initial internal energies have the Boltzmann distribution, the branching fraction $R(E_p)$ of the emerging product ion is expressed as $R(E_p) = \exp((E_p - E_{\rm th})/\langle E_{\rm int}\rangle)$ for $E_p \le E_{\rm th}$, where E_p is the photon energy and $\langle E_{\rm int}\rangle$ is an average internal energy of Cr_3^+. The four onset behaviors in the branching fraction are well explained by using the same fitting parameter of $\langle E_{\rm int}\rangle = 0.079$ eV, as shown by the solid curves. This internal energy corresponds to 306 K, which is consistent with the room temperature of the cluster-growth room. The four threshold energies are thus determined to be 2.00 ± 0.03, 2.18 ± 0.02, 3.75 ± 0.03 and 4.79 ± 0.04 eV, which are denoted by $E_{\rm th1}$ through $E_{\rm th4}$, respectively. Note that the effect of an excited-state lifetime is negligibly small in the present experimental conditions for small clusters; an excess energy necessary for the trimer to dissociate before the secondary mass analysis is estimated to be less than 1 meV in the frame work of the statistical (Rice-Ramsperger-Kassel) theory [9].

2.3 Discussion: photodissociation processes

The photodissociation dynamics of Cr_3^+ is discussed on the basis of the branching fractions shown in Figure 2. In particular, the four threshold energies, $E_{\rm th1} - E_{\rm th4}$, are assigned as follows: the first threshold energy, $E_{\rm th1}$ (2.00 ± 0.03 eV), is ascribed to the process

$$Cr_3^+ \rightarrow Cr^+ + Cr_2. \qquad \text{(i)}$$

This threshold energy is consistent with the one, 1.88 ± 0.10 eV, obtained by the collision-induced-dissociation (CID) experiment [10]. At the second threshold energy, $E_{\rm th2}(2.18 \pm 0.02$ eV), Cr_2^+ production takes over from Cr^+ production. Therefore, $E_{\rm th2}$ is the threshold for

$$Cr_3^+ \rightarrow Cr + Cr_2^+, \qquad \text{(ii)}$$

which is again very close to the CID result (2.01 ± 0.06 eV) [10]. It is thus confirmed that predissociation of

Cr_3^+ occurs at excited states just above the adiabatic dissociation thresholds, which ensures the equivalence of the photodissociation action spectrum to a photoabsorption spectrum above 2.0 eV.

As the photon energy increases, the branching fraction to Cr_2^+ decreases gradually until it turns to increase at about 3.0 eV. This recovery of Cr_2^+ is probably because neutral fragment atoms in excited electronic states come into new dissociation channels:

$$Cr_3^+ \rightarrow Cr^* + Cr_2^+. \qquad \text{(ii*)}$$

Since the first excited states of Cr, ^{5}S, lies 0.94 eV above the ground state, the threshold energy for process (ii*) is 3.12 eV, which coincides with the energy, 3.0 eV, for the recovery of Cr_2^+ mentioned above. Note that the second excited state, ^{5}D, lies above ^{5}S only by 0.02–0.09 eV, which might have a contribution to process (ii*) as well.

The stepwise decrease of the fraction of Cr_2^+ at E_{th3} (3.75 ± 0.03 eV) is due to

$$Cr_3^+ \rightarrow Cr^+ + 2Cr. \qquad \text{(iii)}$$

The dissociation energy of this atomization process is estimated by $E_{th}(Cr...Cr_2^+) + D_0(Cr_2^+)$ to be 3.5–3.6 eV, which is in good agreement with E_{th3}; $E_{th}(Cr...Cr_2^+)$ is equal to E_{th2}, and $D_0(Cr_2^+)$ is reported to be 1.42 ± 0.05 eV by photodissociation spectroscopy [11] and 1.30 ± 0.06 eV by CID [12]. Note that Cr_2^+ is observed at the fraction of about 60% even above the threshold of the atomization process (iii). This means that Cr_2^+ is produced by process (ii*); an excess energy is redistributed to excitation of a Cr atom instead of breaking the chemical bond of Cr_2^+.

Finally, $E_{th4}(4.79 \pm 0.04$ eV) is attributed to the threshold for three-body dissociation including a fragment atom, Cr^*, in an excited state:

$$Cr_3^+ \rightarrow Cr^+ + Cr + Cr^*. \qquad \text{(iii*)}$$

It is explained by the threshold energy for the process (iii) plus the excitation energy of the Cr atom to the ^{5}S state; E_{th3} + 0.94 eV = 4.69 eV.

3 Computational studies

3.1 Computational procedures

Geometry optimization was performed by DFT calculations using the GAUSSIAN 03 program [13]. We used the 6-311+G* basis set. The exchange-correlation term was represented by the BLYP functional [14,15], which is reported to be most feasible to reproduce the properties of the Cr dimer by the recent studies having examined various different functionals for transition-metal dimers [5,6,16,17]; hybrid DFT methods such as B3LYP are problematic, e.g., in that they predict negative values for the binding energy. For the simulation of optical absorption spectra, the transition energies and their oscillator strengths were calculated by the same GAUSSIAN 03 program with the framework of TD-DFT [18–20].

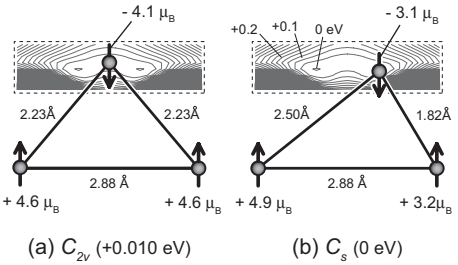

Fig. 3. Geometrical structures optimized by the DFT calculations. The bond lengths and the Mulliken atomic spin densities on each atom are indicated. The contour maps show the potential energy surface for the top apex atom under a constraint that the bond length between the base atoms are fixed at 2.88 Å.

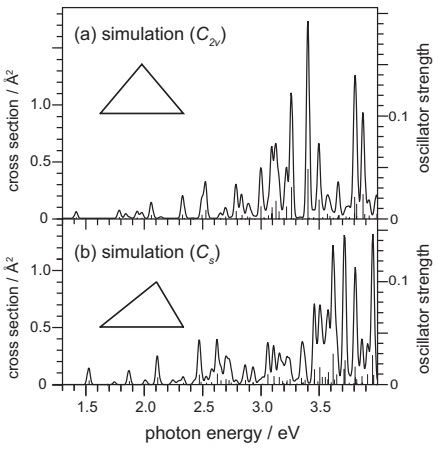

Fig. 4. Simulations of an optical absorption spectrum for (a) the C_{2v} and (b) the C_s structures. Bars indicate the oscillator strengths. The simulated spectra are obtained by adding up all the transitions convoluted with a Gaussian profile of 0.03-eV full-width at half-maximum (FWHM).

3.2 Results of calculations

Figure 3 shows two local-minimum structures obtained by geometry optimization. One has an isoceles triangle structure (C_{2v}) and the other has an asymmetric one (C_s); the latter is more stable only by 0.010 eV. For both the structures, the minimum energies were obtained with $2S + 1 = 6$, where S is the total spin value defined by the difference in number between the majority and the minority spins. We show the Mulliken atomic spin densities on each atomic site in Figure 3, which allow us to gain qualitative insight into the local spin structure and to compare the spin densities with those of Cr_2 [4,21]. The top apex atom couples with the other two atoms in an anti-parallel manner. The Mulliken atomic charge is distributed almost equally on each atom. Figure 4 shows oscillator strengths and simulated optical absorption spectra for the two optimized structures. Many optical transitions are discernible due to excitation of 17 electrons originating from half filled $3d$ and $4s$ orbitals.

3.3 Discussion: structural isomers and chemical bonds

The geometry optimization resulted in two nearly-degenerate structural isomers slightly distorted with each

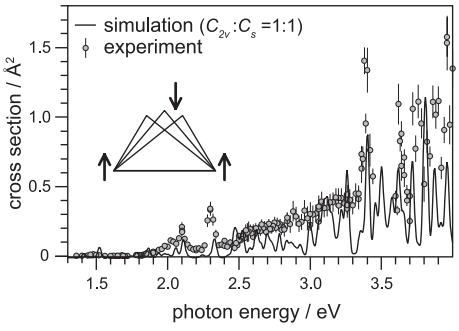

Fig. 5. The total photodissociation cross sections of Cr_3^+ (circles) and the average of the simulated spectra for two optimized structures shown in Figure 4 (solid curve).

other, as shown in Figure 3. The bond lengths of the antiferromagnetic Cr-Cr pairs are 2.23 Å in the C_{2v} structure, while one of them is shortened to 1.82 Å in the C_s structure; accordingly, the local spins on the paired Cr sites are reduced in the latter and are close to the spin densities of $\pm 3.77 \mu_B$ reported for Cr_2 [21]. These features indicate that the contribution of the 3*d* electrons to the bonding of the antiferromagnetic Cr-Cr pair is more significant in the C_s structure than in the C_{2v} structure. This finding is consistent with the properties of the neutral dimer: (1) Cr_2 forms a multiple 3*d*-3*d* bond with a relatively short bond length of 1.6788 Å in the ground $^1\Sigma_g^+$ state [2], which is close to the one (1.82 Å) found in the C_s structure. (2) The potential energy curve of Cr_2 has a double-minimum structure with the primary minimum at 1.6–1.7 Å, corresponding to the bond length above, and the second minimum at between 2 and 3 Å, which is ascribed to formation of 4*s*-4*s* bonding [3,22]. Therefore, it is concluded that the 3*d*-3*d* bonding in the antiferromagnetic Cr-Cr pair gives rise to the stability of the C_s structure, whereas the 4*s*-4*s* bonding operates in the C_{2v} structure. In addition, the bond length, 2.88 Å, between the base atoms in a parallel spin configuration is consistent with the stable bond length of a metastable ferromagnetic dimer, 2.8 Å, reported by a DFT calculation [4].

Since the difference between the two isomers is only the location of the top apex atom, potential energies were calculated as its position was varied. The result is inserted in Figure 3 by contour maps superimposed on the structure. The energy barrier from the C_s to C_{2v} structure was found to be only about 0.02 eV. This barrier height is lower than the zero-point energies, 0.031 eV, calculated for the C_s structure. This indicates that Cr_3^+ has an intrinsically floppy structure with the top apex atom fluctuating around.

The floppiness is manifested in the optical spectrum as well. The photodissociation action spectrum shown in Figure 1c, which is equivalent to an optical absorption spectrum, is reproduced neither by the simulation for the C_{2v} structure (Fig. 4a) nor by the one for the C_s structure (Fig. 4b). However, it was found that the average of the two simulated spectra for the two isomers provides reasonable agreement with the experimental spectrum as shown in Figure 5. The agreement indicates that the electronic structure of the floppy Cr_3^+ is approximated by a mixture of those of the two local minimum structures.

4 Summary

Photodissociation spectroscopy of the Cr_3^+ revealed the threshold excitation energies for several dissociation pathways, which are explained on the basis of energetics. Preferential formation of Cr_2^+ at high energies is associated with an electronically excited Cr atom as a counter product. The DFT calculations suggest a floppy structure slightly distorted from a C_{2v} symmetry, presumably due to competition between 3*d*-3*d* and 4*s*-4*s* bonding natures in the antiferromagnetic Cr-Cr pairs.

The present study was supported by the Special Cluster Research Project of Genesis Research Institute, Inc. The authors gratefully acknowledge SR8000 supercomputing resources from the Center for Computational Materials Science of the Institute for Materials Research, Tohoku University.

References

1. D.L. Michalopoulos, M.E. Geusic, S.G. Hansen, D.E. Powers, R.E. Smalley J. Phys. Chem. **86**, 3914 (1982)
2. V.E. Bondybey, J.H. English, Chem. Phys. Lett. **94**, 443 (1983)
3. M.M. Goodgame, W.A. Goddard III, Phys. Rev. Lett. **54**, 661 (1985)
4. N. Desmarais, F.A. Reuse, S.N. Khanna, J. Chem. Phys. **112**, 5576 (2000)
5. G.L. Gutsev, C.W. Bauschlicher Jr, J. Phys. Chem. A **107**, 4755 (2003)
6. N.E. Schultz, Y Zhao, D.G. Truhlar, J. Phys. Chem. A **109**, 4388 (2005)
7. H. Cheng, L.S. Wang, Phys. Rev. Lett. **77**, 51 (1996)
8. A. Terasaki, S. Minemoto, T. Kondow, J. Chem. Phys. **117**, 7520 (2002)
9. K. Tono, A. Terasaki, T. Ohta, T. Kondow, J. Chem. Phys. **123**, 174314 (2005)
10. C.-X. Su, P.B. Armentrout, J. Chem. Phys. **99**, 6506 (1993)
11. T. Majima, K. Tono, A. Terasaki, T. Kondow, unpublished
12. C.-X. Su, D.A. Hales, P.B. Armentrout, Chem. Phys. Lett. **201**, 199 (1993)
13. M.J. Frisch et al., Gaussian 03, Revision B.04, Gaussian, Inc., Pittsburgh PA, 2003
14. A.D. Becke, Phys. Rev. A **38**, 3098 (1988)
15. C. Lee, W. Yang, R.G. Parr, Phys. Rev. B **37**, 785 (1988)
16. S. Yanagisawa, T. Tsuneda, K. Hirao, J. Chem. Phys. **112**, 545 (2000)
17. C.J. Barden, J.C. Rienstra-Kiracofe, H.F. Schaefer III, J. Chem. Phys. **113**, 690 (2000)
18. R.E. Stratmann, G.E. Scuseria, M.J. Frisch, J. Chem. Phys. **109**, 8218 (1998)
19. R. Bauernschmitt, R. Ahlrichs, Chem. Phys. Lett. **256**, 454 (1996)
20. M.E. Casida, C. Jamorski, K.C. Casida, D.R. Salahub, J. Chem. Phys. **108**, 4439 (1998)
21. K.E. Edgecombe, A.D. Becke, Chem. Phys. Lett. **244**, 427 (1995)
22. S.M. Casey, D.G. Leopold, J. Phys. Chem. **97**, 816 (1993)